assemblage involves archaea in the oxidation of methane. Future studies of environments in which methane is being oxidized anaerobically, combining biomarker techniques and 16S rRNA sequencing, are likely to reveal the identity of the crocetane producer as well as the environmental conditions that determine the growth of either one of these two (or more?) distinct assemblages.

Our results demonstrate the power of complementary information derived from molecular isotopic and phylogenetic lines of evidence. Resolution of the mechanisms by which methane is being oxidized in natural environments is very important both in terms of the global carbon budget and for reconstruction of the relationships between gas-hydrate carbon pools and concentrations of greenhouse gases in ancient atmospheres[28].   □

Methods

Lipid analyses. We extracted free lipids using a Dionex Accelerated Solvent Extraction 200 system at 100 °C and 1000 psi with dichloromethane/methanol (99:1 v/v) as the solvent. We determined the carbon isotopic compositions of total extracts by combustion (sealed quartz tube, CuO/Ag, 850 °C, 8 h) and isotopic mass spectrometry (Micromass Optima). Individual compounds were quantified and identified using an HP 6890 gas chromatograph (GC) equipped with a J&W DB-5 (60-m length, 0.32-mm inner diameter, and 0.25-µm film thickness) capillary column and coupled to an HP 5973 mass-selective detector. Stable carbon isotopic compositions of individual compounds were determined using a Finnigan Delta Plus isotope mass spectrometer coupled to a HP 6890 GC and equipped with a column identical to that described above. Column temperatures were programmed from 40 °C (1 min isothermal) to 130 °C at a rate of 20 °C min^{-1}, and then to 320 °C (60 min isothermal) at 4 °C min^{-1}. We analysed glycerol derivatives as their trimethylsilyl ethers after reaction with BSTFA. Reported δ values are corrected for the introduction of additional carbon atoms by derivatization.

16S rRNA sequencing. We collected subcores at varying sediment depths in sterile tubes, and stored them frozen at −70 °C before nucleic acid extraction. Subsequently, thawed sediment was mixed with an equal volume of lysis buffer (10 mM Tris-HCl pH 8.3, 40 mM EDTA, 750 mM NaCl, 2% sodium dodecyl sulphate), and mechanically disrupted by bead mill homogenization with sterile 0.1 mm zirconium/silica beads. We then purified nucleic acids as previously described[29] by phenol/chloroform (1/1) extraction, chloroform extraction, and subsequent small-scale CsCl density gradient centrifugation. Archaeal or bacterial small-subunit rRNA genes were PCR amplified and cloned using archaeal biased (Ar 20F: TTC CGG TTG ATC CYG CCR G and AR958R: YCC GGC GTT GAM TCC AAT T) or eubacterial biased (Eub27F: AGA GTT TGA TCC TGG CTC AG and 1492R: GGT TAC CTT GTT ACG ACT T) PCR primers as described[30]. Ribosomal RNA clones from each library (bacterial or archaeal) were initially screened by PCR amplification of rDNA plasmid inserts using M13 forward and reverse primers, and subsequent restriction endonuclease digestion using *Hae*III. We analysed restriction fragments by agarose gel electrophoresis on 2.5% NuSieve 3:1 (FMC). Ribosomal RNA clones determined to be unique by RFLP analysis were bidirectionally sequenced using infrared dye-labelled primers and a Licor automated DNA sequencer. Sequences were aligned to a database of rRNA sequences and subsequent bootstrap neighbour-joining analyses performed using Phylip, version 3.5. We calculated evolutionary distances using the Kimura 2-parameter model with a transition/transversion ratio of 2.0.

1. Reeburgh, W. S. in *Microbial Growth on C₁ Compounds* (eds. Lidstrom, M. E. & Tabita, F. R.) 334–342 (Kluwer Academic Publishers, Dordrecht, 1996).
2. Hoehler, T. M. & Alperin, M. J. in *Microbial Growth on C₁ Compounds* (eds. Lidstrom, M. E. & Tabita, F. R.) 326–333 (Kluwer Academic Publishers, Dordrecht, 1996).
3. Brooks, J. M., Field, M. E. & Kennicutt, M. C. II. Observations of gas hydrates in marine sediments, offshore Northern California. *Mar. Geol.* **96**, 103–109 (1991).
4. Hayes, J. M., Freeman, K. H., Popp, B. N. & Hoham, C. H. Compound-specific isotopic analyses: A novel tool for reconstruction of ancient biogeochemical processes. *Org. Geochem.* **16**, 1115–1128 (1990).
5. Pace, N. R. A molecular view of microbial diversity and the biosphere. *Science* **276**, 734–740 (1997).
6. Tornabene, T. G. & Langworthy, T. G. Diphytanyl and dibiphytanyl glycerol ether lipids of methanogenic Archaebacteria. *Science* **203**, 51–53 (1979).
7. Teixidor, P. & Grimalt, J. O. Gas chromatographic determination of isoprenoid alkylglycerol diethers in archaebacterial cultures and environmental samples. *J. Chromatogr.* **607**, 253–259 (1992).
8. Koga, Y., Morii, H., Akagawa-Matsushita, M. & Ohga, M. Correlation of polar lipid composition with 16S rRNA phylogeny in methanogens. Further analysis of lipid component parts. *Biosci. Biotechnol. Biochem.* **62**, 230–236 (1998).
9. Belyaev, S. S. *et al.* Methanogenic bacteria from the Bondyuzhskoe Oil Field: general characterization and analysis of stable-carbon isotopic fractionation. *Appl. Env. Microbiol.* **45**, 691–697 (1983).
10. Irwin, H., Curtis, C. & Coleman, M. Isotopic evidence for source of diagenetic carbonates formed during burial of organic-rich sediments. *Nature* **269**, 209–213 (1977).
11. Freeman, K. H., Hayes, J. M., Trendel, J.-M. & Albrecht, P. Evidence from carbon isotope measurements for diverse origins of sedimentary hydrocarbons. *Nature* **343**, 254–256 (1990).
12. Summons, R. E., Jahnke, L. L. & Roksandic, Z. Carbon isotopic fractionation in lipids from methanotrophic bacteria: Relevance for interpretation of the geochemical record of biomarkers. *Geochim. Cosmochim. Acta* **58**, 2853–2863 (1994).
13. Boone, D. R., Whitman, W. B. & Rouvière, P. in *Methanogens: Ecology, Physiology, Biochemistry, and Genetics* (ed. Ferry J. J.) 35–80 (Chatman & Hall, New York and London, 1993).
14. Munson, M. A., Nedwell, D. B. & Embley, T. M. Phylogenetic diversity of Archaea in sediment samples from a coastal salt marsh. *Appl. Environ. Microbiol.* **63**, 4729–4733 (1997).
15. Hershberger, K. L., Barns, S. M., Reysenbach, A. L., Dawson, S. C. & Pace, N. R. Crenarchaeota in low-temperature terrestrial environments. *Nature* **384**, 420 (1996).
16. Kato, C., Li, L., Tamaoka, J & Horikoshi, K. Molecular analyses of the sediment of the 11000m deep Mariana Trench. *Extremophiles* **1**, 117–123 (1997).
17. McGregor, B. J., Moser, D. P., Alm, E. W., Nealson, K. H. & Stahl, D. A. Crenarchaeota in Lake Michigan sediment. *Appl. Environ. Microbiol.* **63**, 1178–1181 (1997).
18. Vetriani, C., Reysenbach, A. L. & Doré, J. Recovery and phylogenetic analysis of archaeal rRNA sequences from continental shelf sediments. *FEMS Microbiol. Lett.* **161**, 83–88 (1998).
19. Großkopf, R., Stubner, S. & Liesack, W. Novel euryarchaeal lineages detected on rice roots and in anoxic bulk soil of flooded rice microcosms. *Appl. Environ. Microbiol.* **64**, 4983–4989 (1998).
20. Sprott, G. D., Dicaire, C. J., Choquet, C. G., Patel, G. B. & Ekeil, I. Hydroxydiether lipid structures in *Methanosarcina* spp. and *Methanococcus voltae*. *Appl. Environ. Microbiol.* **59**, 912–914 (1993).
21. Zehnder, A. J. B. & Brock, T. D. Methane formation and methane oxidation by methanogenic bacteria. *J. Bacteriol.* **137**, 420–432 (1979).
22. Harder, J. Anaerobic methane oxidation by bacteria employing ^{14}C-methane uncontaminated with ^{14}C-carbon monoxide. *Mar. Geol.* **137**, 13–23 (1997).
23. Hoehler, T. M., Alperin, M. J., Albert, D. B. & Martens, C. S. Field and laboratory studies of methane oxidation in an anoxic marine sediment: Evidence for a methanogen-sulfate reducer consortium. *Glob. Biogeochem. Cycles* **8**, 451–463 (1994).
24. Hansen, L. B., Finster, K., Fossing, H. & Iversen, N. Anaerobic methane oxidation in sulfate depleted sediments: effects of sulfate and molybdate additions. *Aquat. Microb. Ecol.* **14**, 195–204 (1998).
25. Summons, R. E., Franzmann, P. D. & Nichols, P. D. Carbon isotopic fractionation associated with methylotrophic methanogenesis. *Org. Geochem.* **28**, 465–476 (1998).
26. Bian, L. *Isotopic Biogeochemistry of Individual Compounds in a Modern Coastal Marine Sediment (Kattegat, Denmark and Sweden).* Thesis, Indiana Univ. (1994).
27. Holzer, G., Oro, J. & Tornabene, T. G. Gas chromatographic-mass spectrometric analysis of neutral lipids from methanogenic and thermacidophilic bacteria. *J. Chromatogr.* **18**, 795–809 (1979).
28. Kvenvolden, K. A. in *Gas Hydrates: Relevance ot the World Margin Stability and Climate Change* (eds Henriet, J. P. & Mienert, J.) 9–30 (Geological Society, London, 1998).
29. DeLong, E. F. Archaea in coastal marine environments. *Proc. Natl Acad. Sci. USA* **89**, 5685–5689 (1992).
30. Massana, R., Murray, A. E., Preston, C. M. & DeLong, E. F. Vertical distribution and phylogenetic characterization of marine planktonic *Archaea* in the Santa Barbara Channel. *Appl. Environ. Microbiol.* **63**, 50–56 (1997).

Reduced antinociception in mice lacking neuronal nicotinic receptor subunits

Lisa M. Marubio, Maria del Mar Arroyo-Jimenez*, Matilde Cordero-Erausquin, Clément Léna, Nicolas Le Novère, Alban de Kerchove d'Exaerde, Monique Huchet, M. Imad Damaj† & Jean-Pierre Changeux

CNRS UA D1284-"Neurobiologie Moléculaire", Institut Pasteur, 28 rue du Dr Roux, 75724 Paris Cédex 15, France

Nicotine exerts antinociceptive effects by interacting with one or more of the subtypes of nicotinic acetylcholine receptors (nAChRs) that are present throughout the neuronal pathways that respond to pain[1–5]. To identify the particular subunits involved in this process, we generated mice lacking the α4 subunit of the neuronal nAChR by homologous recombination techniques and studied these together with previously generated mutant mice

* Present address: Agrupacion Medicina Enfermezia Humanidades, Dept de Anatomia Humana, 02071 Albacete, Spain.

† Permanent address: Department of Pharmacology, Medical College of Virginia Commonwealth University, Richmond, Virginia 23298-0613, USA.

lacking the β2 nAChR subunit[6]. Here we show that the homozygous α4^{-/-} mice no longer express high-affinity [³H]nicotine and [³H]epibatidine binding sites throughout the brain. In addition, both types of mutant mice display a reduced antinociceptive effect of nicotine on the hot-plate test and diminished sensitivity to nicotine in the tail-flick test. Patch-clamp recordings further reveal that raphe magnus and thalamic neurons no longer respond to nicotine. The α4 nAChR subunit, possibly associated with the β2 nAChR subunit, is therefore crucial for nicotine-elicited antinociception.

The involvement of a particular nAChR subunit in nicotine analgesia has so far been difficult to assess. Pharmacological approaches have indicated a possible contribution of the widely expressed neuronal α4 subunit which co-assembles *in vivo* with the β2 nAChR subunit (and possibly other nAChR subunits) to form high-affinity functional receptors[5,7,8]. By gene targeting and homologous recombination, we have generated a line of mutant mice that lacks the neuronal nAChR α4 subunit (Fig. 1)[6]. Similar to β2^{-/-} mice, mice homozygous for the α4 mutation were born in the expected Mendelian proportion, were capable of reproduction and had no obvious physical abnormalities. In α4^{-/-} mice, no detectable amounts of α4 messenger RNA were found throughout the brain using *in situ* hybridization (Fig. 2a)[9]. Furthermore, there was no significant difference in the expression of the mRNA of the α3, α5, α6, β2 and β4 nAChR subunits or in [¹²⁵I]α-bungarotoxin binding sites (data not shown). Therefore, the disruption of the α4 gene did not cause compensatory changes in the amounts of other nAChR subunit mRNAs or proteins tested.

Autoradiographic ligand-binding experiments with the tritiated forms of two antinociceptive compounds, nicotine and epibatidine, showed that high-affinity binding for these compounds decreased by about 50% in heterozygous α4^{+/-} mice (data not shown) and was absent in most brain regions of α4^{-/-} mice. In α4^{-/-} mice a reduced level of [³H]nicotine binding was detected in the interpeduncular

nucleus (IP) (Fig. 2b, c). [³H]epibatidine binding persisted at high levels in the medial habenula (MHb), superior colliculus (SC) and IP and at low levels in the substantia nigra (SN). However, the residual [³H]nicotine binding in the IP and [³H]epibatidine binding in the SN and SC of α4^{-/-} mice were absent in β2^{-/-} mice[6,7], which indicates that, in these regions, subunits other than α4 form high-affinity nicotine- and epibatidine-binding sites *in situ*, in association with the β2 nAChR subunit. Moreover, the pronounced reduction of [³H]nicotine and [³H]epibatidine binding in α4^{-/-} and β2^{-/-} mice in overlapping regions indicates that these two subunits contribute to most high-affinity nicotinic-binding sites in mouse brain[6,7,10].

We examined several pharmacological responses of α4^{-/-}-mutant mice to the nAChR agonists nicotine and epibatidine and compared these with the effect of nicotine in β2^{-/-} mice. Figure 3 shows the antinociceptive effects of nicotine in hot-plate and tail-flick tests, which distinguish, respectively, between a supraspinal response and a spinal reflex[11,12]. The control latency response to painful stimuli did not differ significantly in wild-type and knockout littermates in
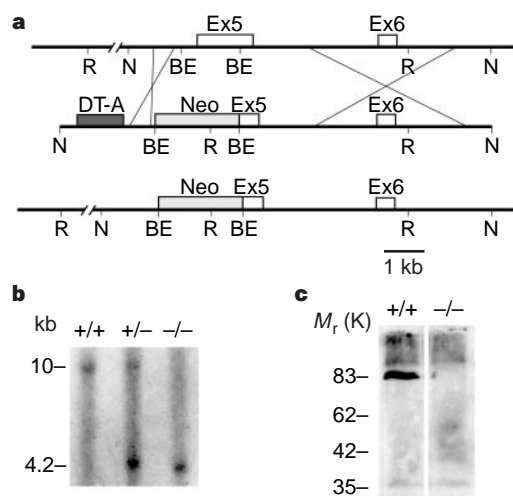

Figure 1 Targeted mutagenesis and expression analysis of the α4 nAChR subunit. **a**, Top, restriction map of the wild-type α4-subunit gene. Ex5, and Ex6 are exon 5 and exon 6 respectively. The portion of exon 5 that was removed is indicated by the two *Bst*EII restriction sites. This fragment contains three of the four putative transmembrane-spanning domains (M1, M2 and M3) and the acetylcholine binding site. Middle, targeting construct used to disrupt the endogenous α4-subunit gene. Neo, the neomycin-resistance gene, replaced part of exon 5. Diptheria toxin-A gene (DT-A)[26] was used to select against random integration. Bottom, structure of the recombined α4 gene. Restriction sites: R, *Eco*RI; N, *Nhe*I; BE, *Bst*EII. **b**, Southern blot analysis of genomic DNA restricted with *Eco*RI from +/+, +/- and -/- mice. **c**, Western blot analysis of total brain extracts using a polyclonal antibody against α4 subunit (M.M.A.-J. *et al.*, submitted).
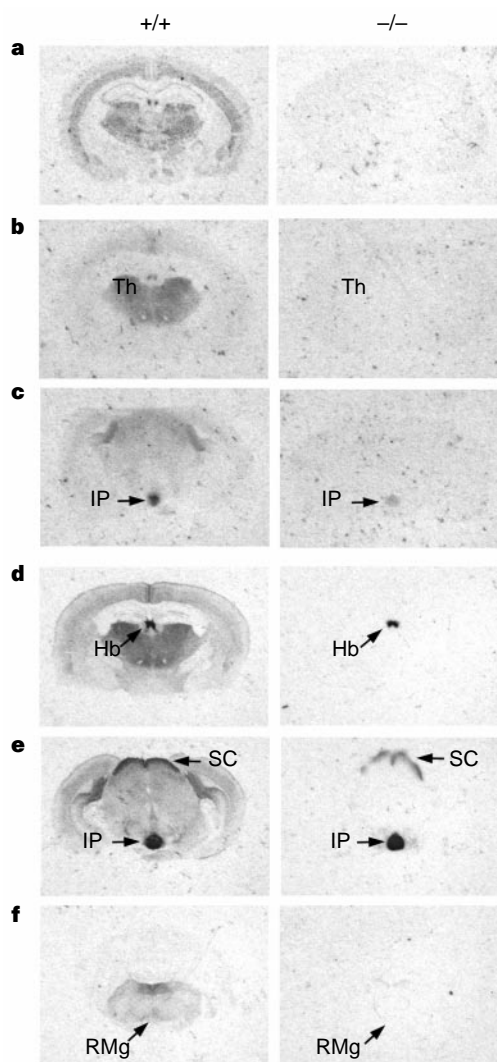

Figure 2 Expression of neuronal nAChRs in mouse brain. **a**, *In situ* hybridization using antisense oligonucleotide probes based on the α4 cDNA sequences. Representative mid-thalamic sections are shown. **b**, **c**, Autoradiographic mapping using [³H]nicotine to reveal the presence of high-affinity nicotine receptors in +/+ and -/- mouse brain sections at Bregma levels of 1.5 and 3.4 mm, respectively. Arrows indicate the IP and show the low levels of binding that persist in the IP in the -/- mice. **d–f**, Autoradiographic mapping using [³H]epibatidine in +/+ and -/- mouse brain sections at Bregma levels of 1.5, 3.4 and 5.8 mm, respectively[27]. Note the binding that remains in the mHb, SC and IP.

either test, indicating that the endogenous activation of either the α4 nAChR subunit or the β2 nAChR subunit is not essential in the perception of acute thermal nociception (Fig. 3a, d). Using the hot-plate test, $\alpha 4^{+/+}$ mice showed a dose-dependent antinociceptive response to nicotine with a median effective dose (ED$_{50}$) of 1.8 mg kg^{-1} (range of confidence limits 1.4–2.4 mg kg^{-1}), a value between the ED$_{50}$ values for the 129 (ED$_{50}$ = 2.2 (2.0–2.5) mg kg^{-1}) or C57Bl/6 (ED$_{50}$ = 1.0 (0.6–1.6) mg kg^{-1}) strains of mice which contribute to the genetic background of the $\alpha 4^{-/-}$ mice (data not shown). For $\beta 2^{+/+}$ mice, the estimated ED$_{50}$ value of 0.93 (0.7–1.3) mg kg^{-1} is close to that of the C57Bl/6 strain which largely contributes to the genetic background of the $\beta 2^{-/-}$ mice. Nicotine-elicited seizures occurred at 3 mg kg^{-1} nicotine in both $\beta 2^{+/+}$ and $\beta 2^{-/-}$ mice, and this dose was

therefore not tested in analgesia experiments. In contrast to wild-type littermates, $\alpha 4^{-/-}$ mice showed no antinociceptive response in the hot-plate test at all doses of nicotine tested (Fig. 3b). Their latency of response was not significantly different from control values regardless of the amount of nicotine injected. $\beta 2^{-/-}$ mice also exhibited a reduced antinociceptive response to all doses of nicotine tested (Fig. 3c). In addition, 9 µg kg^{-1} of epibatidine, a dose that showed a 91 ± 5.8% maximum possible effect (MPE) in C57Bl/6 control mice (data not shown) and 73 ± 15% MPE in $\alpha 4^{+/+}$ mice, showed no antinociceptive effect in $\alpha 4^{-/-}$ mice (Fig. 3g).

In contrast, nicotine was able to cause dose-dependent analgesia in the tail-flick test in $\alpha 4^{+/+}$ and $\alpha 4^{-/-}$ mice and $\beta 2^{+/+}$ and $\beta 2^{-/-}$ mice. However, in both cases the dose–response curve for the
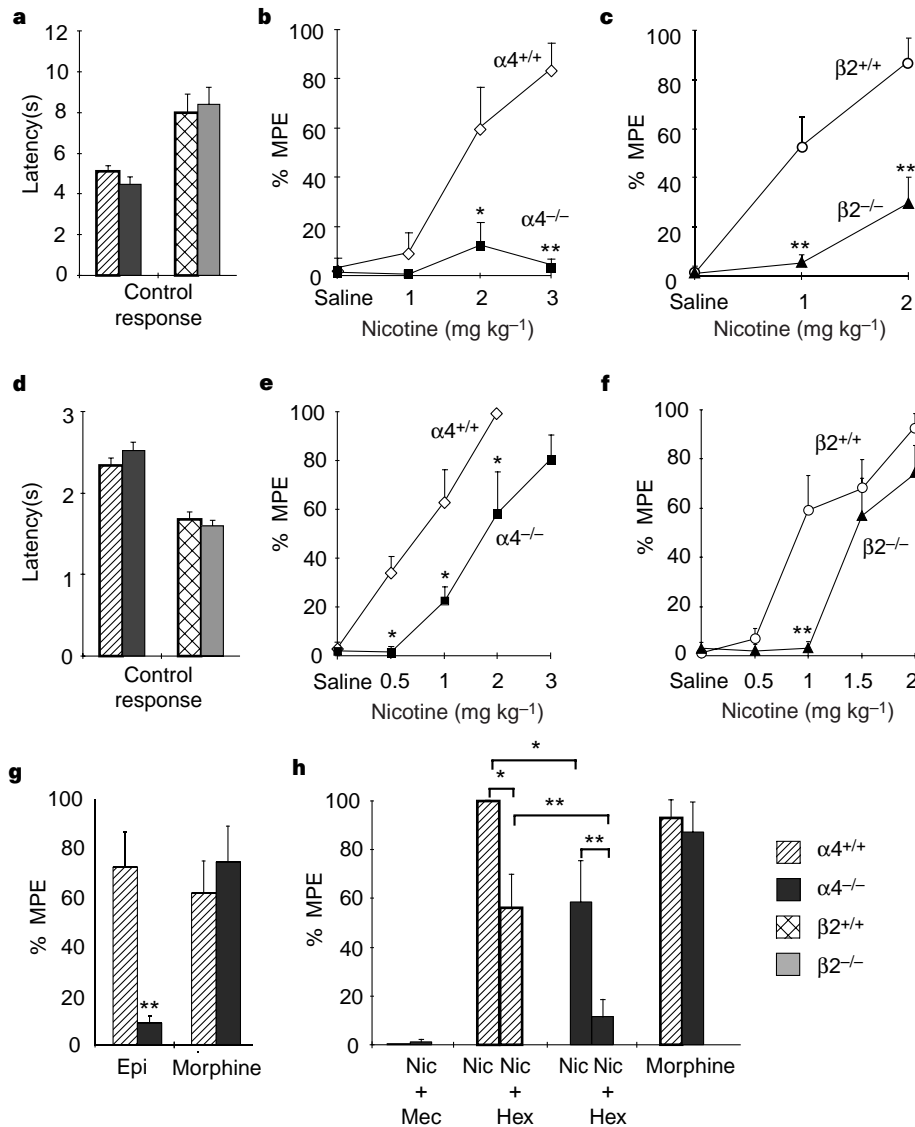

Figure 3 Antinociception of α4-knockout mice in the hot-plate and tail-flick assays. **a**, Pre-test control responses of $\alpha 4^{+/+}$ (n = 38), $\alpha 4^{-/-}$ (n = 40), $\beta 2^{+/+}$ (n = 24) and $\beta 2^{-/-}$ (n = 22) mice on the hot-plate assay. **b**, Antinociception responses in the hot-plate assay to nicotine administration in $\alpha 4^{+/+}$ and $\alpha 4^{-/-}$ littermates using saline (n = 7, 7; +/+, –/–, respectively) and nicotine concentrations of 1 mg kg^{-1} (n = 5, 7), 2 mg kg^{-1} (n = 8, 11) and 3 mg kg^{-1} (n = 8, 8). **c**, Antinociception responses in the hot-plate assay to nicotine administration in $\beta 2^{+/+}$ and $\beta 2^{-/-}$ littermates using saline (n = 5, 6; +/+, –/–, respectively) and nicotine concentrations of 1 mg kg^{-1} (n = 9, 7) and 2 mg kg^{-1} (n = 10, 9). **d**, Pre-test control responses of $\alpha 4^{+/+}$ (n = 40), $\alpha 4^{-/-}$ (n = 42), $\beta 2^{+/+}$ (n = 39) and $\beta 2^{-/-}$ (n = 36) mice in the tail-flick assay. **e**, Antinociception responses in the tail-flick assay to nicotine administration in $\alpha 4^{+/+}$ and $\alpha 4^{-/-}$ littermates using saline (n = 6, 5; +/+, –/–, respectively) and nicotine concentrations

of 0.5 mg kg^{-1} (n = 5, 5), 1 mg kg^{-1} (n = 11, 8), 2 mg kg^{-1} (n = 5, 7) and 3 mg kg^{-1} (n = 5) ($\alpha 4^{-/-}$ only). **f**, Antinociception responses in the tail-flick assay to nicotine administration in $\beta 2^{+/+}$ and $\beta 2^{-/-}$ littermates using saline (n = 6, 5; +/+, –/–, respectively) and nicotine concentrations of 0.5 mg kg^{-1} (n = 8, 5), 1 mg kg^{-1} (n = 9, 9), 1.5 mg kg^{-1} (n = 7, 8) and 2 mg kg^{-1} (n = 9, 8). (Fischer's PLSD, P < 0.01). **g**, Antinociception response in the hot-plate test to 9 µg kg^{-1} epibatidine in $\alpha 4^{+/+}$ (n = 9) and $\alpha 4^{-/-}$ (n = 7) littermates and to 5 mg kg^{-1} morphine in $\alpha 4^{+/+}$ (n = 6) and $\alpha 4^{-/-}$ (n = 5). **h**, Antagonism of antinociception response in the tail-flick assay to 2 mg kg^{-1} nicotine in $\alpha 4^{+/+}$ and $\alpha 4^{-/-}$ littermates using 5 mg kg^{-1} mecamylamine (n = 5, 5) and 5 mg kg^{-1} hexamethonium (n = 8, 7). Antinociception response in the tail-flick assay in $\alpha 4^{+/+}$ (n = 6) and $\alpha 4^{-/-}$ (n = 5) to 5 mg kg^{-1} morphine. Values on the y-axis expressed as mean ±s.e.m. *, P < 0.05; **, P < 0.01. Mec, Mecamylamine; Hex, Hexamethonium.
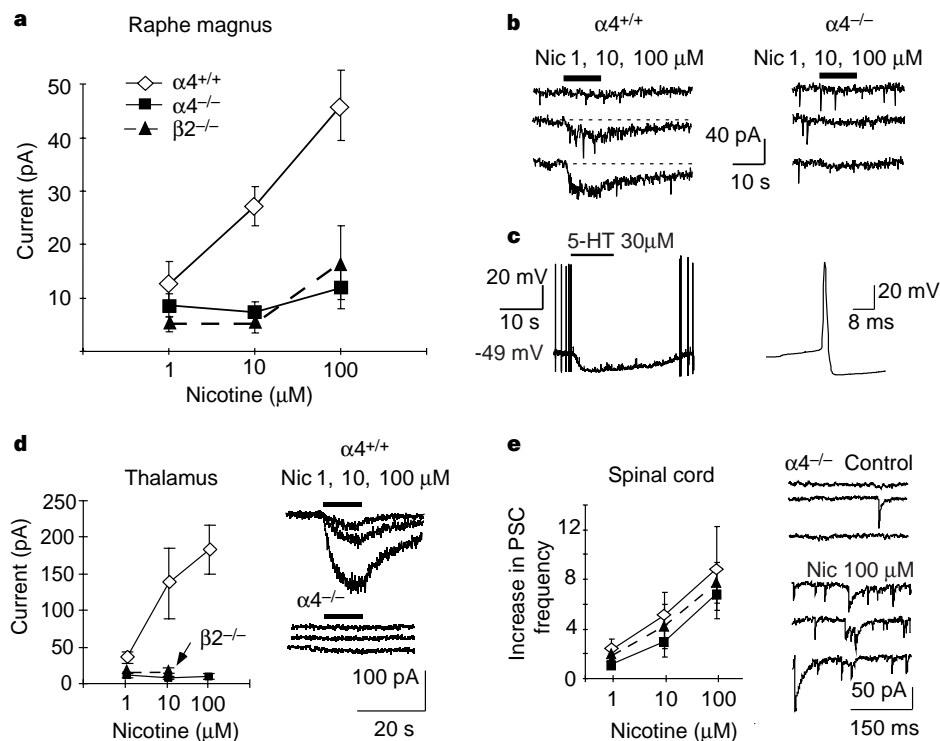
Figure 4 Patch-clamp recordings of nicotine-evoked currents in raphe magnus, thalamus and dorsal horn of the spinal cord of $\alpha4^{+/+}$, $\alpha4^{-/-}$ and $\beta2^{-/-}$ mice. **a**, Dose–reponse curve for nicotine in $\alpha4^{+/+}$, $\alpha4^{-/-}$ and $\beta2^{-/-}$ raphe magnus serotonergic neurons. In $\alpha4^{+/+}$ mice, nicotine concentrations of 10 and 100 μM elicited a significant current in nine out of ten neurons. The non-responding neuron in $\alpha4^{+/+}$ was not included in the dose–response curve. **b**, Nicotine (1–100 μM) elicits an inward current in serotonergic raphe magnus neurons recorded in whole-cell configuration (voltage clamp) in $\alpha4^{+/+}$ but not in $\alpha4^{-/-}$ or $\beta2^{-/-}$ mice. **c**, Serotonin elicits the typical hyperpolarization in serotonergic neurons in the raphe magnus[17] in $\alpha4^{+/+}$ ($n = 10$), $\alpha4^{-/-}$ ($n = 9$) and $\beta2^{-/-}$ ($n = 7$) mice. A representative trace of the response to serotonin (left) and a representative action potential of these neurons (right) are shown. **d**, Dose–response curve for nicotine in the $\alpha4^{+/+}$

($n = 15$ neurons), $\alpha4^{-/-}$ ($n = 11$ neurons) and $\beta2^{-/-}$ ($n = 10$ neurons)[6] antero–ventral thalamus (left). Currents elicited by nicotine in $\alpha4^{+/+}$ thalamic neurons in whole-cell configuration (top, right). No nicotine-elicited current is observed in $\alpha4^{-/-}$ thalamic neurons for 1, 10 or 100 μM nicotine (bottom, right). **e**, Dose–response curve for nicotine-induced increase of PSC frequency in the $\alpha4^{+/+}$ ($n = 8$), $\alpha4^{-/-}$ ($n = 9$) and $\beta2^{-/-}$ ($n = 12$) spinal dorsal horn neurons (layers I–III) (left). Representative traces from an $\alpha4^{-/-}$ neuron before (top, right) and during (bottom, right) application of 100 μM nicotine are shown. Values for all dose–response curves correspond to mean ± s.e.m. of currents recorded at –60 mV. Each point corresponds to the average of four to nine measures. Electrode resistance was 1–2 MΩ for experiments in the raphe magnus and thalamus and 3–5 MΩ in the spinal cord.

mutant mice was shifted to the right ($\alpha4^{+/+}$ $\text{ED}_{50} = 0.7$ (0.5–1.0) mg kg^{-1} compared with $\alpha4^{-/-}$ $\text{ED}_{50} = 1.6$ (1.2–2.1) mg kg^{-1}; $\beta2^{+/+}$ $\text{ED}_{50} = 1.0$ (0.8–1.1) mg kg^{-1} compared with $\beta2^{-/-}$ $\text{ED}_{50} = 1.5$ (1.3–1.7) mg kg^{-1}) (Fig. 3c, f). Thus, both the $\alpha4$ and the $\beta2$ nAChR subunit contribute to the antinociceptive effects of nicotine, although to a larger extent in the hot-plate test, which primarily reflects activation of supraspinal regions.

There were no significant differences between $\alpha4^{+/+}$ and $\alpha4^{-/-}$ mice after morphine administration in both the hot-plate and tail-flick tests (Fig. 3g, h), indicating that opiate analgesia does not depend on activation of $\alpha4$-containing nAChRs[13,14]. In addition, there was no significant difference in non-habituated locomotor activity after injection of 1 or 2 mg kg^{-1} nicotine (data not shown), indicating that the response to nicotine of $\alpha4^{+/+}$ and $\alpha4^{-/-}$ mice and $\beta2^{+/+}$ and $\beta2^{-/-}$ mice in tests for analgesia does not depend only on differences in nicotine-elicited effects on the locomotor system.

The thalamus, raphe magnus, pedunculopontine tegmental nuclei and the dorsal horn of the spinal cord are important in the nicotinic antinociceptive pathways[15,16]. Equilibrium-binding experiments showed the loss of high-affinity nicotine- and epibatidine-binding sites in these areas in $\alpha4^{-/-}$ and $\beta2^{-/-}$ mice (Fig. 2b–f)[6,7]. Consistent with this finding, patch-clamp recordings from serotonergic neurons in the raphe magnus (identified by their response to serotonin)[17] and neurons in the thalamus showed a loss of nicotine-elicited currents in $\alpha4^{-/-}$ and $\beta2^{-/-}$ mice (Fig. 4a–d)[6], indicating a contribution of the $\alpha4$ and $\beta2$ nAChR subunits to

functional receptors in areas implicated in supraspinal nicotine-elicited antinociception[1,13,16]. In contrast, neurons in the superficial layers (I–III) of the dorsal horn of the spinal cord of $\alpha4^{-/-}$ and $\beta2^{-/-}$ mice continued to display a nicotine-elicited, dose-dependent augmentation of the frequency of postsynaptic currents (PSCs) (Fig. 4e).

We then investigated the reasons why the $\alpha4^{-/-}$ mutation only partially reduced the antinociceptive response to nicotinic agonists in the tail-flick test. First, the administration of mecamylamine, a nicotinic antagonist that acts both centrally and peripherally, completely blocked nicotine-elicited antinociception in the tail-flick test (Fig. 3f). Furthermore, previous studies have shown that 5 mg kg^{-1} hexamethonium, a peripheral antagonist that penetrates the blood–brain barrier quite poorly[18], partially blocks the tail-flick response in rats and mice[13,19]. Indeed, in wild-type mice ~50% of the tail-flick response to 2 mg kg^{-1} nicotine was blocked by hexamethonium, in contrast to 80% in $\alpha4^{-/-}$ mice (Fig. 4f). The almost complete block by hexamethonium of the residual antinociception in the knockout mice indicates a contribution of peripheral, non-$\alpha4$ receptors. To identify these peripheral receptors, we performed polymerase chain reaction with reverse transcription (RT-PCR) on complementary DNA from the dorsal root ganglion using degenerative oligonucleotide primers. We observed the expression of $\alpha3$, $\alpha6$, $\alpha7$, $\beta2$ and $\beta4$ subunits in both $\alpha4^{+/+}$ and $\alpha4^{-/-}$ mice, the $\alpha4$ subunit being detected only in the $\alpha4^{+/+}$ mice (data not shown). Immunoprecipitation has shown[20] that most of the nicotinic

receptors in sensory ganglion are composed of $\alpha 3$ and $\beta 4$ subunits, whereas a minority contains $\alpha 4$ and $\beta 2$ subunits. Thus, in the $\alpha 4^{-/-}$ mice $\alpha 3$- and $\beta 4$-subunit-containing nAChRs are likely candidates to mediate the peripheral effects of nicotine in the tail-flick test.

In conclusion, disruption of the $\alpha 4$ and the $\beta 2$ nAChR gene demonstrates that these receptor subunits are an important, although not exclusive, component of the nicotinic pain pathways and most likely cooperate to mediate the antinociceptive effect of nicotine. Specific pharmacological compounds that target these receptors may prove to be therapeutically useful for analgesia. □

....

Methods

Generation of mutant mice. Mouse genomic DNA encoding exon 5 and 6 of the $\alpha 4$ subunit was isolated from a λDASH II male 129 mouse strain genomic library. A DNA construct for homologous recombination was produced by replacing a 1.3 base pair (bp) fragment consisting of a portion of exon 5 and about 400 bp of the upstream intron sequence with a cassette encoding for the neomycin-resistance gene. Transfected embryonic stem-cell colonies that survived after selection with neomycin were subcloned and PCR was used to identify homologously recombined versus randomly integrated DNA. Four positive colonies were isolated and injected into mouse blastocysts. Chimaeric offspring were mated to non-agouti, C57Black/6 mice. Transmission of the mutant $\alpha 4$ gene was indicated by the colour coat marker in approximately 1 out of every 100 of the progeny followed by PCR analysis of DNA isolated from the tail. The positive F1 progeny were crossed with C57Bl/6 mice and their F2 heterozygous offspring were interbred to generate homozygote $\alpha 4^{+/+}$ and $\alpha 4^{-/-}$ littermates. For the generation of $\beta 2^{+/+}$ and $\beta 2^{-/-}$ littermates, F7 (backcrossed with C57Bl/6 for seven generations) heterozygote breeders were used.

Mapping of the neuronal nAChR mRNA in mouse brain. In situ hybridization was performed as described[5]. Oligonucleotides used differing from those previously described are as follows: $\alpha 4$ (mouse) 5′-CTGGGCA-CAGCATTCATACTTCCTGGTGTTGTAGGGTCCCACGGC-3′, 5′-GAAGTC-CAGTTGGTCCACACGGCTGTGCATGCTCACCAA-3′.

Western blot analysis. Whole brain extracts from $\alpha 4^{+/+}$ and $\alpha 4^{-/-}$ mice were homogenized in five volumes of boiling lysis buffer (1% SDS, 10 mM Tris-Cl, pH 7.4) and centrifuged at $550g$ for 10 min. The supernatant was collected, divided into aliquots and frozen at $-80\,°C$ until use. Samples were run on 10% SDS–polyacrylamide gel electrophoresis (SDS–PAGE). The $\alpha 4$-subunit antibody was from Santa Cruz Biotechnology and purified as described (M.M.A.-J. et al., submitted).

Equilibrium binding. Receptor autoradiography was performed as described[7,10]. [³H]nicotine and [³H]epibatidine were obtained from Amersham.

Behavioural analysis. Antinociception was assessed by the tail-flick method as described[21]. A control response (2–6 s) was determined for each animal before treatment and a test latency was determined after drug administration. To minimize tissue damage, a maximum latency of 10 s was imposed. Antagonism studies were done by pretreating the mice subcutaneously with the nicotinic antagonists, mecamylamine or hexamthonium, 10 min before administration of nicotine. The animals were tested 5 min after subcutaneous administration of agonist or 15 min after administration of 5 mg kg^{-1} morphine. Antagonists were administered subcutaneously 15 min before nicotine administration.

Mice were also examined using the hot-plate method (at a temperature of 55 °C). A control response was determined for each animal before treatment. A cut-off time was imposed of 20 s for the $\alpha 4^{+/+}$ and $\alpha 4^{-/-}$ mice and 60 s for $\beta 2^{+/+}$ and $\beta 2^{-/-}$ mice. The nociceptive endpoints in the hot-plate test were hind paw-licking, jumping or rapid thumping of the hind paw. Mice were tested 5 min after subcutaneous injections of nicotine or epibatidine or 20 min after 5 mg kg^{-1} morphine injection for the dose–response evaluation. Some mice were used for both the hot-plate and the tail-flick tests and some $\beta 2^{+/+}$ and $\beta 2^{-/-}$ mice injected with saline or low doses of nicotine were used twice on the tail-flick test. Antinociceptive response was calculated as %MPE, where %MPE $= [(\text{test} - \text{control})/(\text{cut-off} - \text{control})] \times 100$. Experimenters were blind as to the genotype of the mice. After the tail-flick or hot-plate assay, some mice were tested for locomotor activity as described[22].

Data were analysed by an analysis of variance followed by Fisher's post-hoc least significant difference (PLSD) multiple comparison test. The null

hypothesis was rejected at the 0.05 significance level. ED$_{50}$ values with 95% confidence limits for antinociception data were calculated by unweighted least-squares linear regression, as described[23]. Potency ratios were used to compare ED$_{50}$ curves as described[23]. A Student's t-test was used for comparison between individual groups. The ethical guidelines of the International Association for Study of Pain were followed[24].

Patch-clamp recording. Electrophysiolgical experiments were done as previously described[22]. Coronal slices were taken from animals at postnatal day 7–11 (P7–11) for the raphe magnus, P7–14 for the thalamus, and P6–8 for the spinal cord. For the raphe magnus, the intracellular recording solution contained 130 mM KCl, 2 mM MgCl$_2$, 3 mM CaCl, 10 mM EGTA, 4 mM ATP-Na$_2$, 0.4 mM GTP-Na, 10 mM HEPES, pH 7.2. For the spinal cord and thalamus recordings, the intracellular solution contained 140 mM CsCl, 2 mM MgCl, 10 mM BAPTA, 4 mM ATP-Na2, 10 mM HEPES, pH 7.2. Presynaptic responses were analysed as in ref. 25.

RT-PCR. Extraction of total RNA from freshly frozen dorsal root ganglion and spinal cord as a positive control for subunits not expressed in the dorsal root ganglion from $\alpha 4^{+/+}$ and $\alpha 4^{-/-}$ mice was performed using the RNeasy kit (Qiagen, Germany). First-strand cDNA was synthesized with SuperscriptII (Gibco BRL) with random hexamer primers. PCR amplification of nAChRs was done using the following forward oligonucleotide primers: $\alpha 2$ 5′-CTTCTTCACGGGCACTGTGCACTGGGTG-3′, $\alpha 4$ 5′-GTTCTATGACGGAA-GGGTGCAGTGGACA-3′, $\alpha 3$ 5′-ACTCAAGTACACAGGAGAAGTGACT-3′, $\alpha 6$ 5′-TCTTAAGTACGATGGGGTGATAACC-3′, $\alpha 5$ 5′-GATAAAGATTATACGT-GTTCCTTCG-3′, $\beta 3$ 5′-AATTAATTCGATAAAGGTTCCATCA-3′, $\beta 2$ 5′-CTTCTATTCCAATGCTGTGGTCTCCTATG-3′, $\beta 4$ 5′-TGTCTACACCAAC-GTGATTGTGCGTTCCA-3′, $\alpha 7$ 5′-GTGGAACATGTCTGAGTACCCCG-GAGTGAA-3′; and the following reverse oligonucleotide primers: $\alpha 2\alpha 4$ 5′-GGGATGACCAGCGAGGTGGACGGGATGAT-3′, $\alpha 3/\alpha 6$ 5′-TGGTCTCKGT-AATCACCAGSAGAAAGACAGT-3′, $\alpha 5$ 5′-GGCAAAGACAGTCACCATAAT-GGATAGGG-3′, $\alpha 7$ 5′-GAGTCTGCAGGCAGCAAGAATACCAGCA-3′, $\beta 2/\beta 4$ 5′-AGCGGTACGTCGAGGGAGGTGGGAGG-3′, $\beta 3$ 5′-GACCGTGAGAAA-AGACAACCCCAGG-3′. cDNA was amplified for 35 cycles of one minute at each of 96 °C, 60 °C and 72 °C.

1. Iwamoto, E. T. Characterization of the antinociception induced by nicotine in the pedunculopontine tegmental nucleus and the nucleus raphe magnus. *J. Pharmacol. Exp. Ther.* **257,** 120–133 (1991).
2. Bannon, A. W. et al. Broad-spectrum, non-opioid analgesic activity by selective modulation of neuronal nicotinic acetylcholine receptors. *Science* **279,** 77–81 (1998).
3. Spande, T. F. et al. Epibatidine: a novel (chloropyridyl)azabicycloheptaine with potent analgesic activity from an Ecuadoran poison frog. *J. Am. Chem. Soc.* **114,** 3475–3478 (1992).
4. Wada, E. et al. Distribution of $\alpha 2$, $\alpha 3$, $\alpha 4$, and $\beta 2$ neuronal nicotinic receptor subunit mRNAs in the central nervous system: a hybridization histochemical study in the rat. *J. Comp. Neurol.* **284,** 314–335 (1989).
5. Le Novère, N., Zoli, M. & Changeux, J. P. Neuronal nicotinic receptor $\alpha 6$ subunit mRNA is selectively concentrated in catecholaminergic nuclei of the rat brain. *Eur. Neurosci.* **8,** 2428–2439 (1996).
6. Picciotto, M. et al. Abnormal avoidance learning in mice lacking functional high-affinity nicotine receptor in the brain. *Nature* **374,** 65–67 (1995).
7. Zoli, M., Léna, C., Picciotto, M. R. & Changeux, J. P. Identification of four classes of brain nicotinic receptors using $\beta 2$ mutant mice. *J. Neurosci.* **18,** 4461–4472 (1998).
8. Ramirez-Latorre, J. et al. Functional contributions of $\alpha 5$ subunit to neuronal acetylcholine receptor channels. *Nature* **380,** 347–351 (1996).
9. Le Novère, N. & Changeux, J. P. Molecular evolution of the nicotinic acetylcholine receptor: an example of multigene family in excitable cells. *J. Mol. Evol.* **40,** 155–172 (1995).
10. Clarke, P. B. S., Schwartz, R. D., Paul, S. M., Pert, C. B. & Pert, A. Nicotinic binding in rat brain: autoradiographic comparison of ³H-acetylcholine, ³H-nicotine, and ¹²⁵I-α-bungarotoxin. *J. Neurosci.* **5,** 1307–1315 (1985).
11. D'Amour, F. E. & Smith, D. L. A method for determining loss of pain sensation. *J. Pharmacol. Exp. Ther.* **72,** 74–79 (1941).
12. Caggiula, A. R., Epstein, L. H., Perkins, K. A. & Saylor, S. Different methods of assessing nicotine-induced antinociception may engage different neural mechanisms. *Physchopharmacology* **122,** 301–306 (1995).
13. Tripathi, H. L., Martin, B. R. & Aceto, M. D. Nicotine-induced antinociception in rats and mice: correlation with nicotine brain levels. *J. Pharmacol. Exp. Ther.* **221,** 91–96 (1982).
14. Sahley, T. L. & Bernston, G. G. Antinociceptive effects of central and systemic administration of nicotine in the rat. *Psychopharmacology* **65,** 279–283 (1979).
15. Jurna, I., Krauss, P. & Baldauf, J. Depression by nicotine of pain-related nociceptive activity in the rat thalamus and spinal cord. *Clin. Pharmacol.* **72,** 65–73 (1993).
16. Bitner, R. S. et al. Role of the nucleus raphe magnus in antinociception produced by ABT-594: immediate early gene responses possibly linked to neuronal nicotinic acetylcholine receptors on serotonergic neurons. *J. Neurosci.* **18,** 5426–5432 (1998).
17. Pan, Z. Z., Wessendorf, M. W. & Williams, J. T. Modulation by serotonin of the neurons in the rat nucleus raphe magnus in vitro. *Neuroscience* **54,** 421–429 (1993).
18. Asghar, K. & Roth, L. J. Entry and distribution of hexamethonium in the central nervous system. *Biochem. Pharmacol.* **20,** 2787–2795 (1971).
19. Rao, T. S., Correa, L. D., Reid, R. T. & Lloyd, G. K. Evaluation of anti-nociceptive effects of neuronal nicotinic acetylcholine receptor (NAChR) ligands in the rat tail-flick assay. *Neuropharmacology* **35,** 393–405 (1996).

20. Flores, C. M., DeCamp, R. M., Kilo, S., Rogers, S. W. & Hargreaves, K. M. Neuronal nicotinic receptor expression in sensory neurons of the rat trigeminal ganglion: demonstration of α3β4, a novel subtype in the mammalian nervous system. *J. Neurosci.* **16**, 7892–7901 (1996).
21. Damaj, M., Patrick, G., Creasy, K. & Martin, B. Pharmacology of lobeline, a nicotinic receptor ligand. *J. Pharmacol. Toxicol.* **282**, 410–419 (1997). **(AUTHOR: journal title OK?)**
22. Picciotto, M. R. *et al.* Acetylcholine receptors containing the β2 subunit are involved in the reinforcing properties of nicotine. *Nature* **391**, 173–177 (1998).
23. Tallarida, R. & Murray, R. *Manual of Pharmacological Calculations with Computer Programs* (Springer, New York, 1987).
24. Zimmerman, M. Ethical guidelines for investigations of experimental pain in conscious animals. *Pain* **16**, 109 (1983).
25. Léna, C. & Changeux, J. P. Role of Ca²⁺ ions in nicotinic facilitation of GABA release in mouse thalamus. *J. Neurosci.* **17**, 576–585 (1997).
26. Yagi, T. *et al.* A novel negative selection for homologous recombinants using diphtheria toxin A fragment gene. *Anal. Biochem.* **214**, 77–86 (1993).
27. Franklin, K. B. J. & Paxinos, G. *The Mouse Brain in Stereotaxic Coordinates* (Academic, San Diego, 1997).

Tbx5 and *Tbx4* genes determine the wing/leg identity of limb buds

Jun K. Takeuchi*†, **Kazuko Koshiba-Takeuchi***†, **Ken Matsumoto***, **Astrid Vogel-Höpker**‡, **Mayumi Naitoh-Matsuo***, **Keiko Ogura***, **Naoki Takahashi***, **Kunio Yasuda*** & **Toshihiko Ogura***

* *Nara Institute of Science and Technology Graduate School of Biological Sciences 8916-5, Takayama, Ikoma, Nara, 630-0101 Japan*
‡ *Max-Planck Institute for Brain Research, Deutschordenstr. 46, 60528 Frankfurt/M., Germany*
† *These authors contributed equally to this work.*

....

Much progress has been made in understanding limb development[1–3]. Most genes are expressed equally and in the same pattern in the fore- and hindlimbs, which nevertheless develop into distinct structures[3–8]. The T-box genes *Tbx5* and *Tbx4*, on the other hand, are expressed differently in chick wing (*Tbx5*) and leg (*Tbx4*) buds[9–12]. Molecular analysis of the *optomotor blind* gene[13], which belongs to the same family of transcription factors, has revealed that this gene is involved in the transdetermination of *Drosophila* wing and leg imaginal discs[14]. In addition, expression of *Tbx5* and *Tbx4* correlates well with the identity of ectopic limb buds induced by fibroblast growth factor[4,5,15–19]. Thus, it is thought that *Tbx5* and *Tbx4* might be involved in determining limb identity. Another candidate is the *Pitx1* gene, which encodes a bicoid-type homeodomain transcription factor that is expressed in leg buds[20,21]. Here we determine the importance of these factors in establishing limb identity.

To introduce foreign complementary DNA efficiently into chick embryonic cells, we adopted a novel *in ovo* electroporation system[22]. In a conventional replication-competent avian sarcoma (RCAS) retrovirus system, there is a time lag (of about 16 h) between injection of the virus and full gene expression[23]. This could prevent the conversion of wing/leg identity, because limb identity seems to be determined and fixed at early stages (stages 10 to 12)[24,25]. To overcome this problem, we electroporated RCAS retrovirus plasmids directly into the prospective limb-bud fields. In this system, gene expression starts immediately after electroporation (within 2 h[22]). In addition, subsequent production and infection of the recombinant retrovirus fix, expand and maintain the expression in limb buds. We used this system to express Tbx5/Tbx4 ectopically in limb fields at stages 7 to 9.
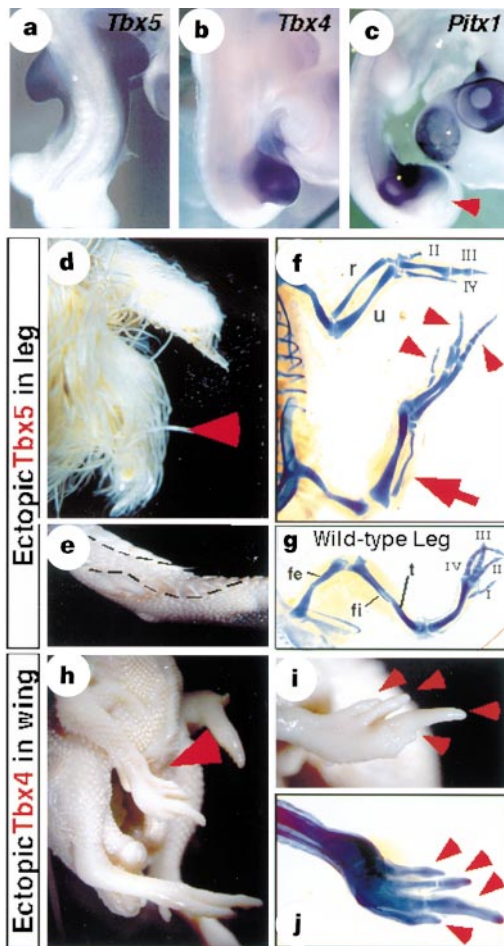

Figure 1 Misexpression of Tbx5 and Tbx4 converts the wing/leg identity of limb buds. **a**–**c**, Normal expression patterns of *Tbx5* (**a**), *Tbx4* (**b**) and *Pitx1* (**c**) genes at stage 23. **d**–**f**, Tbx5 misexpressed leg. Leg ectoderm is covered by feathers (**d**, red arrowhead). Fibula is elongated and makes a joint at its distal end like a normal ulna (**f**). **e**, Partial scale-to-feather conversion in the area indicated by broken lines. **g**, Skeletal pattern of the normal leg. **h**–**j**, Tbx4 misexpressed wings. The wing was elongated and four separated digits were formed with claws (red arrowheads, **i**). Four digits and a thin ulna are observed (red arrowheads, **j**). r, radius; u, ulna; fe, femur; fi, fibula; t, tibia; I–IV, digits.

When a fusion construct containing *Tbx5* and the enhanced green fluorescent protein gene (RCASBP–*Tbx5*–EGFP) was electroporated into the leg fields of chick embryos, several mesodermal and ectodermal phenotypes were observed in 15% ($n = 519$) of electroporated legs (Fig. 1d–f). The fibula, which is normally short (Fig. 1g) and does not articulate with the metatarsal bones, was elongated, and clearly articulated with metatarsal bones (red arrow in Fig. 1f), although it did not articulate correctly with the femur and was thinner than a normal ulna. The number of phalanges was different from in a normal wing, but there were only three digits, as in normal wings (arrowheads in Fig. 1f). Thus, misexpression of Tbx5 in the leg can induce wing-like skeletal patterns, albeit partially. Ectodermal phenotypes were also converted. Figure 1d shows an electroporated leg which is completely covered in feathers (red arrowhead), without any scales. Partial scale-to-feather conversion is shown in Fig. 1e: in this case, scales were completely replaced with feathers in the leg area (dashed lines). These results indicate that misexpression of the *Tbx5* gene in the embryonic chick leg induces a partial wing-like morphology, with three digits, elongation of the fibula and scale-to-feather conversion.

We also induced misexpression of Tbx4 in the wing fields. When RCASBP–*Tbx4*–EGFP was electroporated into the prospective